Atomic Data and Nuclear Data Tables 154 (2023) 101586

Contents lists available at ScienceDirect

Atomic Data and Nuclear Data Tables

journal homepage: www.elsevier.com/locate/adt

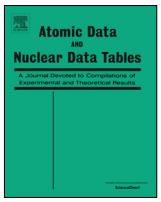

Electron scattering cross sections for the ground and excited states of tin

Haadi Umer [a,*], Yuri Ralchenko [b], Igor Bray [a], Dmitry V. Fursa [a]

[a] Department of Physics and Astronomy, Curtin University, Perth 6102, Australia
[b] National Institute of Standards and Technology, Gaithersburg MD 20899, USA

ARTICLE INFO

Article history:
Received 13 April 2023
Accepted 8 May 2023
Available online 26 May 2023

Keywords:
Tin
Electron scattering
Excitation
Ionisation
Rate coefficients

ABSTRACT

A comprehensive set of cross sections for electron scattering from the ground and first four excited states of tin has been calculated using the Relativistic Convergent Close-Coupling method. Elastic scattering, momentum transfer, total scattering, and total-inelastic scattering cross sections have been produced for the $5p^2\ ^3P_{0,1,2}$, $^1D_2$ and $^1S_0$ states of atomic tin over a projectile energy range of 0.1 eV to 1000 eV. Over the same projectile energy range, state-resolved cross sections for excitations to the $5p^2$, $5p6s$, $5p5d$ and $5p6p$ manifolds from the ground and first four excited states of tin are presented. Total single-ionisation cross sections have been calculated which account for the direct ionisation of electrons in the valence $5p$ and closed $5s$ shells, as well as indirect contributions from excitation auto-ionisation. These ionisation cross sections are presented for projectile energies up to 1000 eV. Maxwellian rate coefficients have been calculated for all studied transitions over electron temperatures ranging from 0.5 eV to 200 eV and fitted with simple formulas. The fit coefficients are tabulated for use in modelling applications.

* Corresponding author.
E-mail address: haadi.umer@postgrad.curtin.edu.au (H. Umer).

https://doi.org/10.1016/j.adt.2023.101586
0092-640X/

Contents

1. Introduction

Extensive electron collision datasets for tin have recently become in demand for various plasma modelling applications, particularity in fusion research and nano-lithography. In tokamak fusion reactors such as ITER, bombardment of the plasma-facing components during operation will lead to erosion and damage [1]. This is especially a concern for the divertor region of such fusion reactors, and the lifetime of the divertors will strongly be determined by this erosion [2,3]. One method to monitor this damage is to include a tin marker within the plasma-facing components which will only enter the plasma after a pre-determined amount of damage is sustained from erosion. Tin is also presently the primary candidate material for use in liquid metal divertors for the European DEMO fusion reactor, which promises to be a major improvement over the tungsten mono-block design of the ITER divertor [4]. Extreme-ultraviolet (EUV) lithography is an advanced microchip manufacturing technique which relies on a tin plasma to generate the 13.5 nm light used to imprint structures on semiconducting materials [5,6]. However, the details on the origins of this light from the tin plasma are not well understood. In both fusion and lithography applications, comprehensive and reliable data for electron collisions with tin are important for the accurate modelling of plasmas involving tin.

Comprehensive electron collision datasets for tin in literature are sparse. Excitation cross sections for transitions within the $5p^2$ ground electron configuration were first studied by Srivastava et al. [7] as part of a larger study in which they considered a few of the Group IV elements. They utilised the relativistic distorted wave (RDW) method to calculate differential cross sections (DCS) for transitions from the $^3P_0$ ground state to the $^3P_1$, $^3P_2$ and $^1D_2$ low-lying excited states at projectile energies of 25 eV and 40 eV. Excitations from the $5p^2\ ^3P_0$ ground state to the $5p6s\ ^3P^\circ_0$, $^3P^\circ_1$, $^3P^\circ_2$ and $^1P^\circ_1$ excited states were calculated by Sharma et al. [8] using the RDW method. They presented DCS at 20 eV, 50 eV, 80 eV and 100 eV and also presented integrated cross sections (ICS) for transitions from the $5p^2\ ^3P_{0,1,2}$, $^1D_2$ and $^1S_0$ states to all states in the $5p6s$ manifold for projectile energies ranging from 5 eV to 100 eV. Transitions to this manifold are important as the $5p6s$ states lie low in the tin spectrum and include dipole allowed transitions from the ground and first four excited states. Both Srivastava et al. [7] and Sharma et al. [8] had no previous data to compare with.

Ionisation of neutral tin has been studied once experimentally and several times theoretically. Freund et al. [9] measured the single-ionisation cross section of tin in a larger study which included many atomic targets. Poor agreement was found with theoretical results available then for tin and there were no other measurements to compare with. Theoretical predictions for electron-impact single ionisation of tin were first produced by McGuire [10] using the generalised-oscillator-strength form of the Born approximation, which is accurate only at large projectile energies. Bartlett and Stelbovics [11] presented ionisation cross sections for tin as part of a comprehensive study on a large number of atoms, in which the Born approximation was utilised. More accurate treatment of ionisation of tin was performed by Kim and Stone [12] who applied the binary-encounter Bethe approximation (BEB) to calculate direct ionisation of the valence $5p$ and closed $5s$ shells, and also calculated contributions from excitation auto-ionisation using a scaled plane-wave Born approach. Good agreement was found with the measurements of Freund et al. [9] by both Bartlett and Stelbovics [11] and Kim and Stone [12]. The semi-relativistic configuration-averaged distorted-wave (CADW) method was utilised by Loch et al. [13] to calculate electron-impact ionisation cross sections for all ion stages in the Sn isonuclear sequence, including neutral tin. Their results included contributions to the total ionisation cross section (TICS) from direct ionisation and indirect ionisation through excitation to auto-ionising states. They compared their results with the measurements of Freund et al. [9] and found the CADW results to overestimate at the peak as was expected for a distorted-wave approximation applied to a neutral system. Total ionisation of Sn was also studied by Naghma et al. [14] who first calculated the total inelastic cross section using the spherical complex optical potential (SCOP) method, and then produced the total ionisation cross section from the inelastic one by applying the complex scattering potential-ionisation contribution (CSP-ic) method. They found good agreement with the results of [9–11].

Here, we present a comprehensive cross section dataset for electron scattering on the ground and first four excited states of tin calculated using the Relativistic Convergent Close-Coupling (RCCC) method. This dataset includes integrated cross sections for elastic scattering, excitations, total and total-inelastic scattering (TCS and inelastic-TCS), and ionisation. This is a unitary formalism, which ensures that all of these collision processes are coupled. Cross sections are presented over projectile energies spanning from 0.1 eV to 1000 eV for all processes. State-resolved excitation cross sections for transitions from states in the ground $5p^2$ electron configuration to all states in the $5p6s$, $5p5d$ and $5p6p$ manifolds are presented. Excitation and super-elastic cross sections for transitions within the $5p^2$ manifold are also included. Maxwellian rate coefficients are calculated using the RCCC cross

sections for electron temperatures ranging from 0.5 eV to 200 eV. These rates are fitted to an analytical expression for which coefficients are provided. In our recent study of this system [15], we presented excitation cross sections for scattering on the $^3P_0$ ground state alongside elastic scattering, momentum transfer and ionisation cross sections for the ground and first four excited states. Here we extend the results of [15] to larger energies and evaluate cross sections for excitations from excited states. This establishes a comprehensive set of cross sections for electron collisions with neutral tin.

2. Calculation details

2.1. Structure calculations

Tin is an open-shell atom with a sufficiently large mass such that its energy levels exhibit fine-structure splitting. We model it as two $5p$ electrons over an inert Dirac–Fock core. All orbitals from $1s^2$ up to $5s^2$ are taken as the core, and the corresponding wave functions for these orbitals are obtained using the GRASP [16] package. One-electron polarisation potentials are included to better model the target structure, in which the j-dependent fall-off radii are chosen to fit the experimental energy levels of Sn. This polarisation potential is similar to the one described by Bray [17], and the static dipole polarisability of Sn^{2+} required for this model is taken as 17.75 a_0^3 [18]. The Sn^+ quasi one-electron Dirac–Fock Hamiltonian is diagonalised in a L-spinor basis [19] to produce one-electron functions for the $s_{1/2}$ to $g_{9/2}$ symmetries. For each symmetry, 20 one-electron orbitals are then included in standard two-electron configuration-interaction (CI) calculations [20] to produce two-electron configurations for Sn. Both frozen-core and correlation configurations are included in our calculations, which are chosen to best model both the bound and the continuum spectrum of tin. Frozen core configurations are of the form $5p_{1/2}nl_j$ and $5p_{3/2}nl_j$ where nl_j are the one-electron functions generated from the Sn^+ diagonalisation. Correlation configurations are of the form $nl_jn'l'_{j'}$ where orbitals are restricted to $ns_{1/2}$ for $n = 6, 7$, and $np_{1/2,3/2}$, $nd_{3/2,5/2}$ for $n = 5, 6$. CI coefficients are obtained through the diagonalisation of the Sn Dirac-Hamiltonian in a basis constructed from the generated one-electron orbitals. A large number of target states are produced with total angular momentum ranging from $J = 0$ to $J = 6$ for negative and positive parities, which include both bound and continuum pseudo-states. A two-electron polarisation potential [21] is used to improve the calculated optical oscillator strength (OOS) for the resonance transition $5p^2\ ^3P_0 \rightarrow 5p6s\ ^3P_1$ and bring it closer to the value of 0.20 as recommended by NIST [22]. The RCCC structure calculations in this way produce a value of 0.211. The converged value for the static dipole polarisability of tin as given by the RCCC structure model is 37.94 a_0^3. This is smaller than the accurate value of 52.9 a_0^3 calculated by [23] as it does not include contributions from inner core excitations.

2.2. Relativistic Convergent Close-Coupling method

The RCCC method has already been well documented in literature [24–26] and the calculations performed for this dataset were identical to the ones performed in [15]. From the two-electron configurations built in the structure calculations for tin, scattering models with differing numbers of included states are produced. These models include the first 33, 75, 152, 237, 399 and 482 generated target states and are denoted by RCCC(33), RCCC(75), RCCC(152), RCCC(237), RCCC(399) and RCCC(482), respectively. These subsets of target states are used to perform the close-coupling expansion of the total scattering wave-function, and the larger models lead to increasingly converged results. A partial-wave expansion is utilised to solve the partial-wave form of the relativistic Lippmann–Schwinger equation for each total angular momentum J and parity Π of the electron-tin scattering system. The T-matrix elements are obtained and used to calculate integrated cross sections for various transitions. Partial-waves with total angular momentum ranging from $J = 1/2$ to $J = 41/2$ for negative and positive parities are included in the scattering calculations. An analytical Born subtraction technique is applied to increase the rate of partial-wave convergence. The various RCCC models are then combined to produce cross sections for elastic scattering and excitations. At low projectile energies the RCCC(33) and RCCC(75) models are utilised while the larger models are adopted for higher energies. To deal with numerical instabilities in the calculations at low projectile energies, smoothing techniques are applied to the cross sections which are discussed in [15].

For the calculation of total single-ionisation cross sections, contributions from the direct ionisation (DI) of the valence $5p$, core $5s$ and indirect excitation auto-ionisation must be included. Firstly, the large RCCC models described above are used to produce the $5p$ direct ionisation cross section for each initial target state $5p^2\ ^3P_{0,1,2}$, $^1D_2$ and $^1S_0$. In order to correctly estimate these $5p$ DI cross sections, extrapolation of the RCCC cross sections using large Born calculations is required. First-order Born direct ionisation calculations are performed using a structure model which included states with large total angular momenta and energies. This model is too large to be included in the full RCCC calculations as the computational resources required would be unfeasible. These Born calculations are then used to extrapolate the RCCC(482) DI cross section to account for the high-lying, large angular-momentum continuum pseudo-states which were not present in the RCCC(482) scattering model. A detailed description of this scaling is given in [15].

The RCCC calculations for the direct ionisation of the $5s$ electrons proceed in a similar manner. A structure model is first produced in which the $5p$ electrons are fixed in a closed $5p^2_{1/2}$ configuration and one-electron excitations are allowed out of the $5s^2$ shell. Multiple models with 59, 85, 161 and 263 states are produced to calculate the $5s$ DI cross section and test for convergence. Same as in the $5p$ case, Born calculations using a large structure model are performed to extrapolate the $5s$ DI cross section and account for high angular momentum and energy pseudo-states missing in the smaller RCCC models. Further details on these calculations are given in [15]. Contributions from the indirect excitation auto-ionisation process are taken from the scaled plane-wave Born calculations performed by [12]. The total-ionisation cross section (TICS) is produced for each initial target state by adding the corresponding RCCC $5p$ DI, RCCC $5s$ DI and scaled plane-wave Born excitation auto-ionisation cross sections.

3. Cross sections

Integrated cross sections for electron scattering on the ground and first four excited states of tin are presented for elastic scattering, momentum transfer, excitations to the $5p^2$, $5p6s$, $5p5d$ and $5p6p$ manifolds, total and total-inelastic scattering, and ionisation. The studied target states in each manifold and their energies are listed in Table A. All excitation cross sections are state resolved. We have also produced cross sections summed over excitations to the $5p5d$ and $5p6p$ manifolds. For dipole allowed transitions with relatively large OOS values, integrated cross sections are scaled using the accurate optical oscillator strengths of Oliver and Hibbert [27] as described in [15]. RCCC OOS values calculated for all studied dipole allowed transitions are presented in Table B alongside comparison with those of Oliver and Hibbert [27].

Table A
States in each manifold of the tin spectrum studied in this paper and their excitation energies (in eV) relative to the ground state.

Manifold	State	RCCC	NIST[22]
$5p^2$	$^3P_0$	0.000	0.000
	$^3P_1$	0.210	0.210
	$^3P_2$	0.440	0.425
	$^1D_2$	1.159	1.068
	$^1S_0$	2.345	2.128
$5p6s$	$^3P^\circ_0$	4.293	4.295
	$^3P^\circ_1$	4.324	4.329
	$^3P^\circ_2$	4.814	4.789
	$^1P^\circ_1$	4.881	4.867
$5p5d$	$^3F^\circ_2$	5.416	5.416
	$^3F^\circ_3$	5.546	5.527
	$^3D^\circ_2$	5.581	5.473
	$^3D^\circ_1$	5.675	5.518
	$^3F^\circ_4$	5.946	5.965
	$^1D^\circ_2$	5.965	5.845
	$^3D^\circ_3$	6.053	5.888
	$^3P^\circ_2$	6.178	6.034
	$^3P^\circ_1$	6.221	6.073
	$^3P^\circ_0$	6.255	6.136
	$^1F^\circ_3$	6.262	6.186
	$^1P^\circ_1$	6.349	6.215
$5p6p$	$^3D_1$	5.275	5.250
	$^3P_1$	5.411	5.377
	$^3D_2$	5.415	5.385
	$^3P_0$	5.474	5.430
	$^1P_1$	5.835	5.778
	$^3D_3$	5.877	5.828
	$^3P_2$	5.917	5.856
	$^3S_1$	5.987	5.927
	$^1D_2$	6.041	5.975
	$^1S_0$	6.205	6.126

Table B
OOS values for dipole allowed transitions from the ground and first four excited states of tin. The asterisk (*) indicates the transitions for which the RCCC cross sections are scaled using the Oliver and Hibbert [27] OOS values.

Initial State	Final State	RCCC	Oliver and Hibbert[27]
$5p^2\ ^3P_0$	$5p6s\ ^3P^\circ_1$ *	2.11×10^{-1}	2.051×10^{-1}
	$5p6s\ ^1P^\circ_1$ *	7.70×10^{-2}	6.042×10^{-2}
	$5p5d\ ^3D^\circ_1$ *	5.53×10^{-1}	3.884×10^{-1}
	$5p5d\ ^3P^\circ_1$	1.15×10^{-3}	
	$5p5d\ ^1P^\circ_1$	8.69×10^{-2}	
$5p^2\ ^3P_1$	$5p6s\ ^3P^\circ_0$ *	9.42×10^{-2}	8.802×10^{-2}
	$5p6s\ ^3P^\circ_1$ *	5.29×10^{-2}	5.137×10^{-2}
	$5p6s\ ^3P^\circ_2$ *	1.25×10^{-1}	1.102×10^{-1}
	$5p6s\ ^1P^\circ_1$ *	1.25×10^{-2}	1.112×10^{-2}
	$5p5d\ ^3F^\circ_2$	3.84×10^{-3}	
	$5p5d\ ^3D^\circ_2$ *	2.47×10^{-1}	2.130×10^{-1}
	$5p5d\ ^3D^\circ_1$ *	6.23×10^{-2}	5.203×10^{-2}
	$5p5d\ ^1D^\circ_2$	1.53×10^{-1}	1.186×10^{-2}
	$5p5d\ ^3P^\circ_2$	4.29×10^{-2}	
	$5p5d\ ^3P^\circ_1$	1.13×10^{-1}	
	$5p5d\ ^3P^\circ_0$	4.42×10^{-2}	
	$5p5d\ ^1P^\circ_1$	3.50×10^{-3}	
$5p^2\ ^3P_2$	$5p6s\ ^3P^\circ_1$ *	8.66×10^{-2}	7.798×10^{-2}
	$5p6s\ ^3P^\circ_2$ *	1.92×10^{-1}	1.785×10^{-1}
	$5p6s\ ^1P^\circ_1$ *	3.29×10^{-4}	3.641×10^{-4}
	$5p5d\ ^3F^\circ_2$	1.53×10^{-2}	
	$5p5d\ ^3F^\circ_3$ *	1.29×10^{-1}	1.701×10^{-1}
	$5p5d\ ^3D^\circ_2$ *	2.63×10^{-3}	2.650×10^{-3}
	$5p5d\ ^3D^\circ_1$	1.25×10^{-4}	4.634×10^{-5}
	$5p5d\ ^1D^\circ_2$ *	1.48×10^{-2}	1.231×10^{-2}
	$5p5d\ ^3D^\circ_3$ *	2.94×10^{-1}	1.103×10^{-1}
	$5p5d\ ^3P^\circ_2$	1.35×10^{-1}	
	$5p5d\ ^3P^\circ_1$	3.70×10^{-2}	
	$5p5d\ ^1F^\circ_3$	2.90×10^{-2}	
	$5p5d\ ^1P^\circ_1$	6.79×10^{-4}	
$5p^2\ ^1D_2$	$5p6s\ ^3P^\circ_1$ *	2.87×10^{-2}	2.520×10^{-2}
	$5p6s\ ^3P^\circ_2$ *	1.93×10^{-2}	1.551×10^{-2}
	$5p6s\ ^1P^\circ_1$ *	1.81×10^{-1}	1.746×10^{-1}
	$5p5d\ ^3F^\circ_2$	2.78×10^{-2}	1.628×10^{-2}
	$5p5d\ ^3F^\circ_3$	2.62×10^{-2}	1.667×10^{-2}
	$5p5d\ ^3D^\circ_2$	4.15×10^{-2}	4.727×10^{-3}
	$5p5d\ ^3D^\circ_1$	3.27×10^{-3}	4.728×10^{-3}
	$5p5d\ ^1D^\circ_2$ *	4.92×10^{-2}	4.102×10^{-2}
	$5p5d\ ^3D^\circ_3$	1.76×10^{-3}	3.369×10^{-2}
	$5p5d\ ^3P^\circ_2$	3.91×10^{-2}	2.868×10^{-2}
	$5p5d\ ^3P^\circ_1$	1.73×10^{-3}	1.382×10^{-5}
	$5p5d\ ^1F^\circ_3$ *	3.07×10^{-1}	2.854×10^{-1}
	$5p5d\ ^1P^\circ_1$	3.40×10^{-3}	9.482×10^{-3}
$5p^2\ ^1S_0$	$5p6s\ ^3P^\circ_1$ *	7.97×10^{-3}	7.458×10^{-3}
	$5p6s\ ^1P^\circ_1$ *	7.37×10^{-2}	8.350×10^{-2}
	$5p5d\ ^3D^\circ_1$	3.92×10^{-2}	1.709×10^{-2}
	$5p5d\ ^3P^\circ_1$	2.51×10^{-2}	3.690×10^{-2}
	$5p5d\ ^1P^\circ_1$ *	3.82×10^{-1}	3.382×10^{-1}

Cross sections for transitions from the excited $5p^2\ ^3P_{1,2}$, $^1D_2$ and $^1S_0$ states to all states in the $5p6s$ manifold are presented in Fig. 1 alongside comparison with the RDW results of Sharma et al. [8]. Similar to what was found for the ground $^3P_0$ state [15], agreement with the RDW results at low to intermediate projectile energies is poor. The behaviour of the cross sections for both RCCC and RDW at high projectile energies is similar for all of the transitions, even if the agreement in the magnitude is not good. Cross sections for the dipole allowed transitions are relatively large at high projectile energies. The dipole forbidden transitions have cross sections that quickly decrease with increasing projectile energy. The disagreement between the RCCC and the RDW results at low and intermediate projectile energies is due to the RDW method being a high-energy approximation.

Figs. 2 and 3 present the total excitation cross sections summed over all states in the $5p5d$ and $5p6p$ manifolds from the excited $5p^2\ ^3P_{1,2}$, $^1D_2$ and $^1S_0$ states of neutral tin. Generally, the summed cross sections for excitations to states in the $5p5d$ manifold are larger and dominated by dipole allowed transitions in the intermediate to high energy range. In contrast, the $5p6p$ ones have sharp peaks with magnitudes a little smaller than the $5p5d$ ones, and then all of them decrease quickly with increasing projectile energy. This is because all transitions to states in the $5p6p$ manifold are dipole forbidden. No other data is available to compare with for these cross sections.

Fig. 4 has the total and total-inelastic cross sections for electron scattering from the first four excited states of tin. The TCS includes elastic scattering, excitations, super-elastic transitions, and ionisation. The inelastic-TCS includes all the same contributions as the TCS except elastic scattering. From these figures, it is clear that elastic scattering dominates the cross section in the low to intermediate projectile electron energy range.

The total single-ionisation cross section for the ground and first four excited states is presented in Fig. 5 alongside comparison with experiment and other theoretical results. The measurements of Freund et al. [9] agree best with the RCCC TICS for the $5p^2\ ^1D_2$ target state over most of the projectile energy range. This agreement, alongside the experimental ionisation onset beginning before the ground state ionisation threshold of 7.344 eV, indicates that some fraction of the experimental target tin atoms were initially in excited states. The CADW [13] cross section is for the ground state of tin and includes contributions from the DI of the $5p$, $5s$, $4d$ and $4p$ subshells and also from excitation autoionisation of the $5s$, $4d$ and $4p$ subshells. This result overestimates

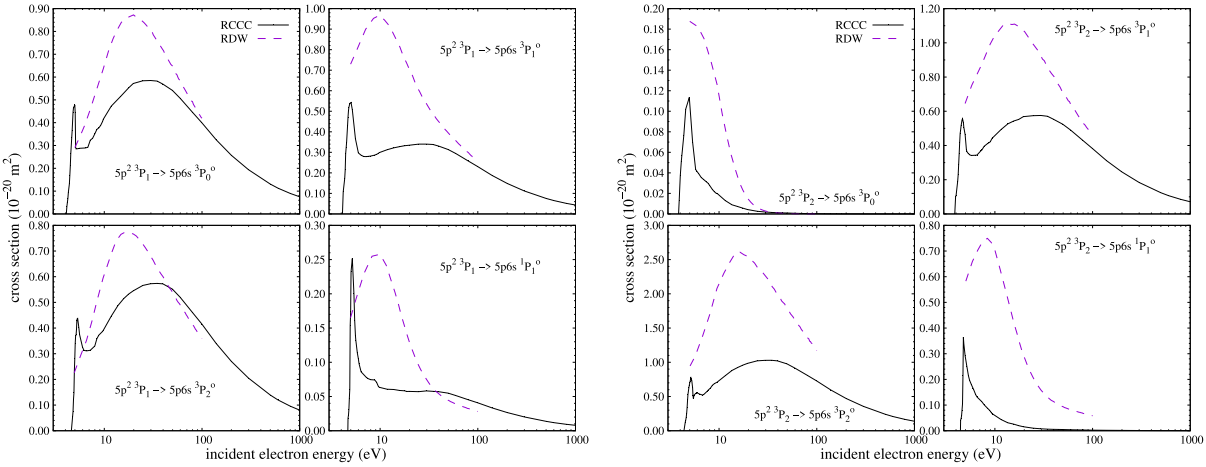

(a) Excitations from $5p^2\ ^3P_1$

(b) Excitations from $5p^2\ ^3P_2$

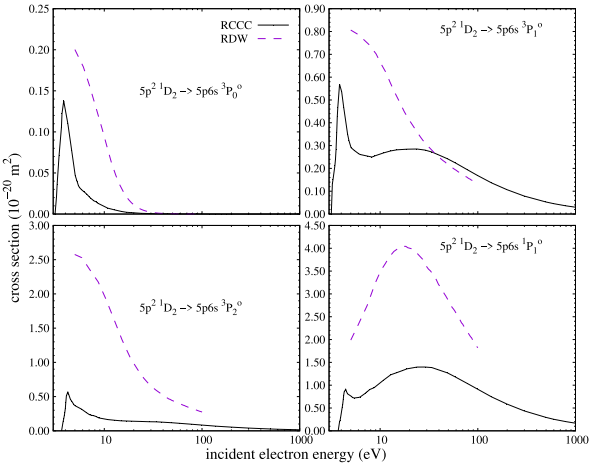

(c) Excitations from $5p^2\ ^1D_2$

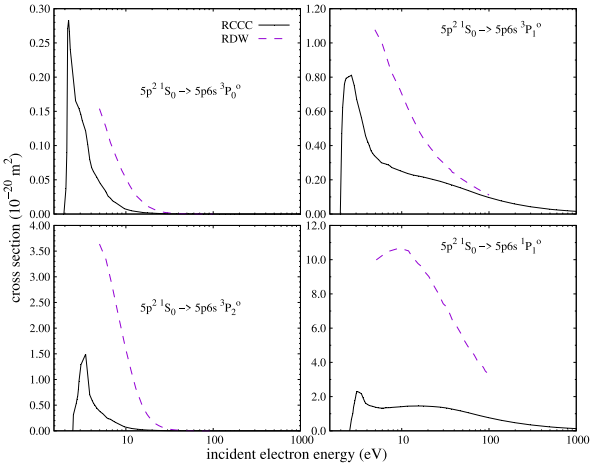

(d) Excitations from $5p^2\ ^1S_0$

Fig. 1. Cross sections for excitations to the 5*p*6*s* manifold from the first four excited states of tin (solid curves). RDW results of Sharma et al. [8] (dashed curves) are also presented.

the experiment and is larger than all other theories in the low to intermediate projectile energy range. This behaviour is expected as CADW is a first order calculation and only accurate at high energies. The SCOP CSP-ic [14] cross section is calculated for the ground state. It underestimates the measurements before the peak, and has good agreement with the experiment at higher projectile energies. This result also has reasonable agreement with RCCC at low to intermediate projectile energies, however, for energies above 200 eV the SCOP CSP-ic results are larger than the present RCCC cross sections. The peaks of all the RCCC TICS are shifted to higher projectile energies (at about 45 eV) compared to the other theoretical and experimental results (which have peaks at about 30 eV).

4. Maxwellian rate coefficients

Maxwellian rate coefficients are calculated using the cross sections for each transition presented in this study. The RCCC cross sections are first interpolated, and then used to calculate the rate coefficients over temperatures ranging from 0.5 eV to 200 eV using Eq. (1). This temperature range is chosen because it is where neutral tin typically exists in plasmas.

$$\langle \sigma_{f,i} v \rangle = \frac{8\pi}{\sqrt{m_e}} \left(\frac{1}{2\pi k_B T} \right)^{3/2} \int_0^\infty \sigma_{f,i}(E) e^{-E/k_B T} E \mathrm{d}E. \tag{1}$$

Here, the $k_B T$ is the electron temperature, $\langle \sigma_{f,i} v \rangle$ is the rate coefficient (in which $\sigma_{f,i}$ is the cross section and v is the atomic velocity), $k_B = 8.617 \times 10^{-5}$eV K^{-1} is the Boltzmann constant, $m_e = 0.511$ MeV/c^2 is the electron mass, and i and f refer to the initial and final states of the scattering system. These rate coefficients are then fitted to an analytical function of temperature using the formula

$$\langle \sigma_{f,i} v \rangle = A_0^2 \exp\left(-\frac{A_1}{(k_B T)^{A_2}} \right) \times \left(\frac{A_3}{(k_B T)} + \frac{A_4}{(k_B T)^2} + \frac{A_5}{(k_B T)^3} \right) (k_B T)^{A_6}. \tag{2}$$

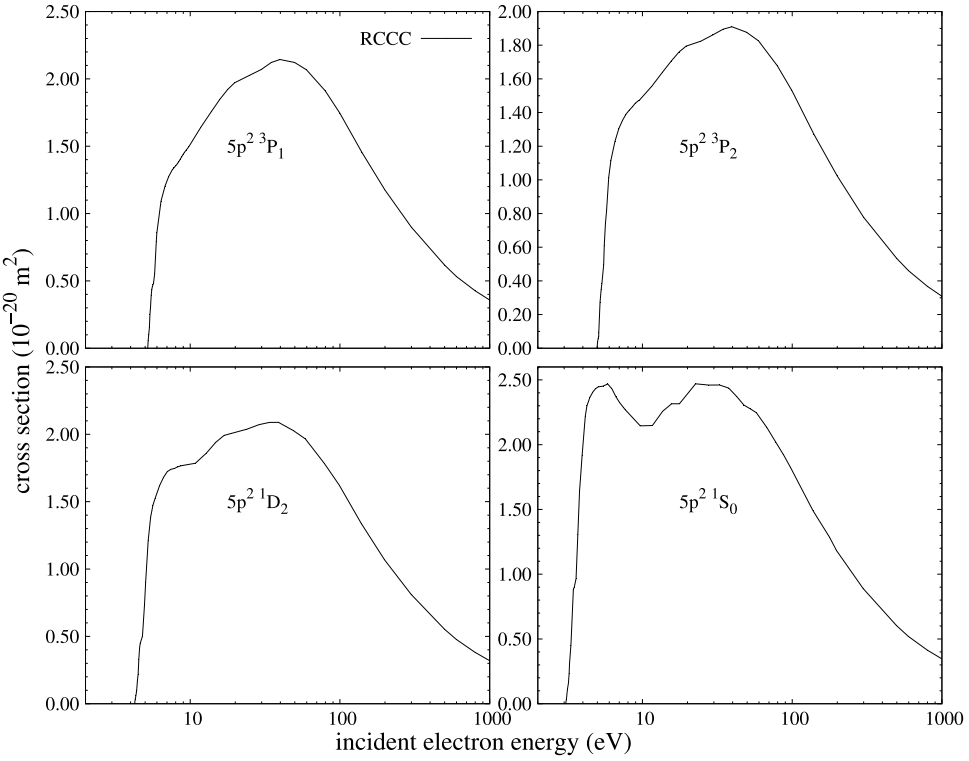

Fig. 2. Integrated cross sections for excitations from the first four excited states of tin to all states in the 5*p*5*d* manifold.

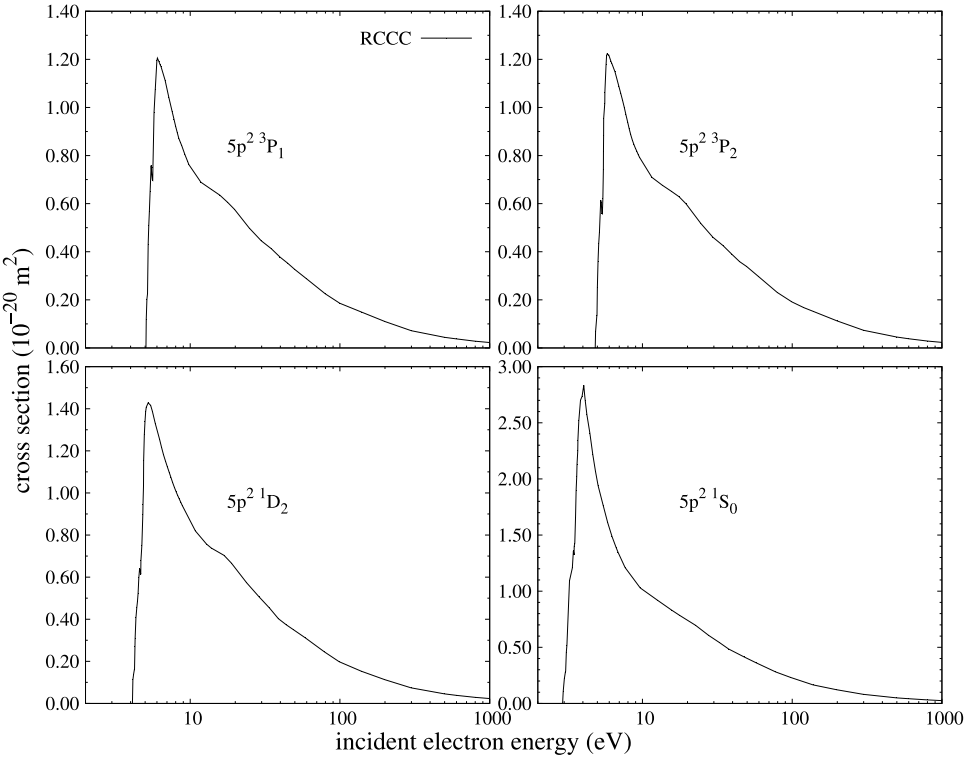

Fig. 3. Integrated cross sections for excitations from the first four excited states of tin to all states in the 5*p*6*p* manifold.

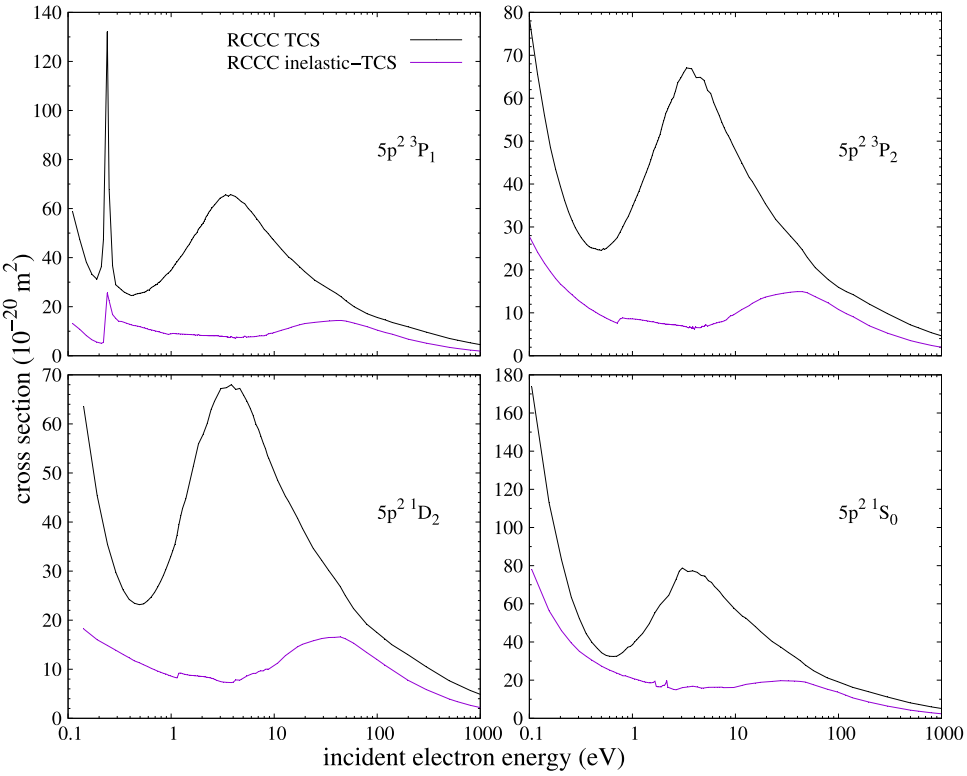

Fig. 4. Total and total-inelastic scattering cross sections from the first four excited states of tin.

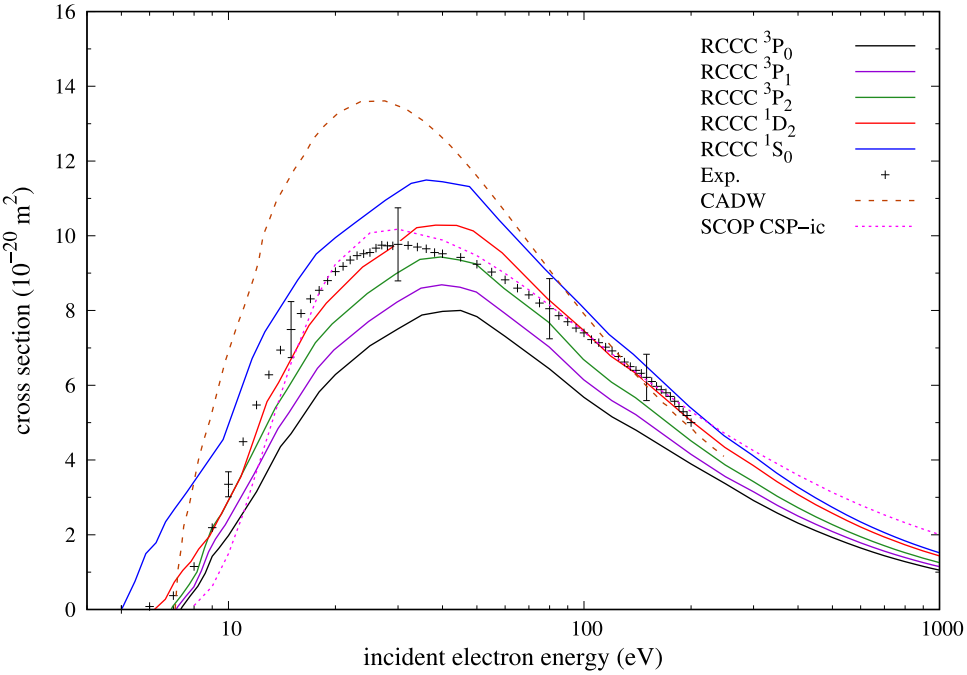

Fig. 5. Total single-ionisation cross sections for the ground and first four excited states of tin. Includes comparison with CADW [13], SCOP CSP-ic [14] and experiment [9].

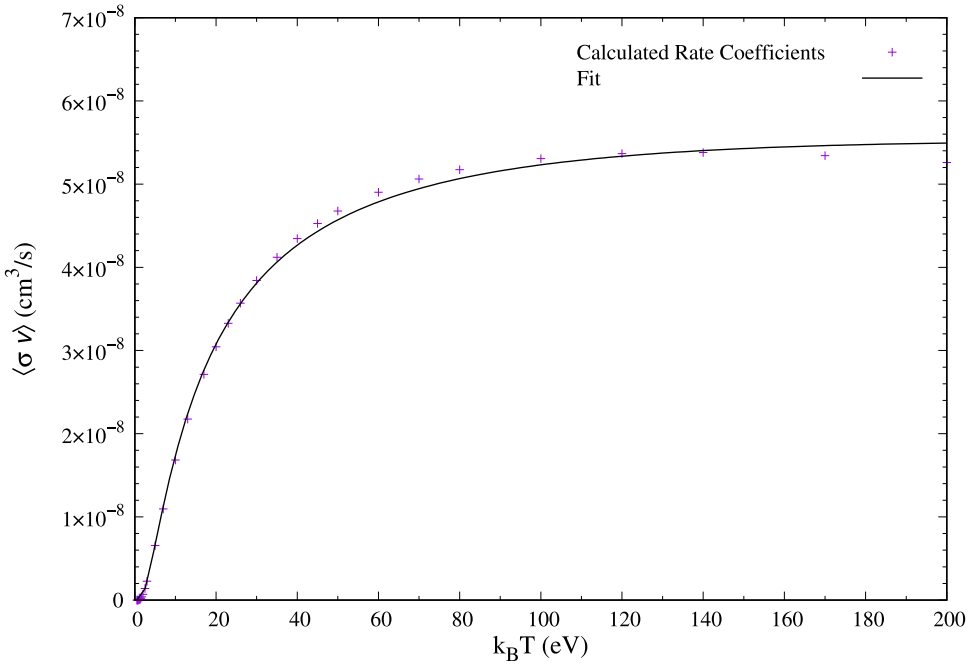

Fig. 6. Illustration of the fitting done for the rate coefficients to Eq. (2) as a function of electron temperature. Shown here for the transition $5p^2\ ^3P_0 \rightarrow 5p5d\ ^3D^\circ_1$.

The fits are performed using the fitting parameters A_0, A_1, A_2, A_3, A_4, A_5 and A_6 for each transition. Fig. 6 illustrates the fitting performed on the numerically calculated rate coefficients using Eq. (1) to the formula in Eq. (2) for the $5p^2\ ^3P_0 \rightarrow 5p5d\ ^3D^\circ_1$ transition. The quality of the fits for other transitions is similar. As neutral tin exists only at low temperatures in the majority of plasmas, the accuracy of the fits at lower temperatures was prioritised.

5. Access to the data

All data files are part of the supplementary material for this paper. There is a subdirectory for each initial target state for which data is presented in this study. These are named

- `5p2_3P0/`
- `5p2_3P1/`
- `5p2_3P2/`
- `5p2_1D2/`
- `5p2_1S0/`

Each data file in these subdirectories includes the integrated cross section as a function of projectile electron energy, the fitting parameters for the rate coefficients and a header providing details on the data. The datafile naming convention is shown below.

- Elastic scattering integrated cross sections:
  `RCCC-e-Sn-[i.c]_[i.t]_ELASTIC_ICS.txt`
- Elastic scattering momentum-transfer cross sections:
  `RCCC-e-Sn-[i.c]_[i.t]_ELASTIC_MTCS.txt`
- State-to-state transition cross sections:
  `RCCC-e-Sn-[i.c]_[i.t]-[f.c]_[f.t].txt`
- Summed cross sections:
  `RCCC-e-Sn-[i.c]_[i.t]-[f.c]_SUMMED.txt`
- Total cross sections:
  `RCCC-e-Sn-[i.c]_[i.t]_TCS.txt`
- Total-inelastic cross sections:
  `RCCC-e-Sn-[i.c]_[i.t]_inelTCS.txt`
- Ionisation cross sections:
  `RCCC-e-Sn-[i.c]_[i.t]_TICS_TOTAL.txt`

Here, `i.c` and `f.c` refer to the initial and final electron configurations, respectively, and `i.t` and `f.t` refer to the initial and final terms of the states, respectively. An example of each type of file name is provided below.

- Elastic scattering integrated cross section for scattering from the $5p^2\ ^3P_1$ state:
  `RCCC-e-Sn-5p2_3P1_ELASTIC_ICS.txt`
- Elastic scattering momentum-transfer cross section for scattering from the $5p^2\ ^1D_2$ state:
  `RCCC-e-Sn-5p2_1D2_ELASTIC_MTCS.txt`
- Cross section for excitation from the $5p^2\ ^1S_0$ state to the $5p6p\ ^1P_1$ state:
  `RCCC-e-Sn-5p2_1S0-5p6p_1P1.txt`
- Cross section summed over all excitations to states in the $5p5d$ manifold from the $5p^2\ ^3P_2$ state:
  `RCCC-e-Sn-5p2_3P2-5p5d_SUMMED.txt`
- Total cross section for scattering from the $5p^2\ ^3P_1$ state:
  `RCCC-e-Sn-5p2_3P1_TCS.txt`
- Total-inelastic cross section for scattering from the $5p^2\ ^3P_1$ state:
  `RCCC-e-Sn-5p2_3P1_inelTCS.txt`
- Ionisation cross section for the $5p^2\ ^3P_0$ state:
  `RCCC-e-Sn-5p2_3P0_TICS_TOTAL.txt`

Below is an example of the form the RCCC-e-Sn-5p2_3P0-5p5d_3D1.txt data file.

```
# Wed 22 Mar 2023 12:46:06 AWST
# Relativistic Convergent Close Coupling method for electron collisions with atomic tin.
# Reference: Umer et al., Atom. Data. Nucl. Data Tables (2023)
#
# Data in this file is for the transition:  5p^2 3P0 -> 5p5d 3D1
#
# Integrated cross sections are in atomic units (a.u.) and given as a function of projectile
# energy measured in eV.
#
# Maxwellian rate coefficients are provided in analytical form using the following equation:
#   RATE_C(X) = a0**2*EXP(-a1/X**a2)*(a3/X + a4/X**2 + a5/X**3)*X**a6
# The components of this equation are:
#   - RATE_C(X): rate coefficient in cm^3/s as a function of X
#   - X: electron temperature (k_B T) in eV
#   - a0-a6: fitting parameters.
# These rate coefficients are only valid for a temperature range (k_B T) of 0.5 to 200 eV.
#
# Fitting parameters for the rate coefficients:
#  a0 = 2.4476e-06 , a1 = 7.4897e+00 , a2 = 6.1351e-01 , a3 = 2.8454e+04 , a4 = -2.6059e+04 ,
a5 = 6.1751e+03 , a6 = 8.4191e-01
#
# SCALED using OOS value published by Oliver (see paper for discussion); RCCC value = 0.553,
Oliver value = 0.388
# The scaling was done as follows: CS_scaled = CS_RCCC * OOS_Oliver/OOS_RCCC
# Reference: Oliver, P.; Hibbert, A., J. Phys. B At. Mol. Opt. Phys. 2008, 41, 165003.
#
# energy (eV) | integrated cross section (a.u.)
  5.6700E+00 0.0000E+00
  5.8000E+00 1.7294E-01
  6.2000E+00 3.9944E-01
  ...     ...
```

6. Conclusions

A large dataset of 185 integrated cross sections has been produced for electron scattering from the ground and first four excited states of neutral tin. These include cross sections for elastic scattering, excitations to the $5p^2$, $5p6s$, $5p5d$ and $5p6p$ manifolds, total scattering, total inelastic scattering and ionisation. The calculations were performed with the Relativistic Convergent Close-Coupling method, and results have been produced for projectile energies ranging from 0.1 eV to 1000 eV for elastic scattering, excitations and ionisation. Maxwellian rate coefficients are also presented for all processes studied in this paper for electron temperatures ranging from 0.5 eV to 200 eV. The present excitation cross sections have been compared with RDW [8] and agreement was found to be poor at low to intermediate projectile energies and slightly better at high projectile energies. There was good agreement in the behaviour and shape of the RCCC and RDW cross sections at high energies. The differences between the two sets of results were attributed to the fact that the RDW method is a first-order calculation and only accurate at high projectile energies. The RCCC total single-ionisation cross sections were compared with experiment [9] and other calculations [13,14]. Reasonable agreement was found with experiment and SCOP CSP-ic [14]. Agreement with CADW [13] was poor as it is considerably larger than RCCC over the low to intermediate projectile energy range. The RCCC TICS for the $^1D_2$ excited state best agreed with experiment but the RCCC peak was slightly shifted towards higher energies compared to the experimental one.

Declaration of competing interest

The authors declare that they have no known competing financial interests or personal relationships that could have appeared to influence the work reported in this paper.

Data availability

The data is part of the supplementary material for this paper

Acknowledgments

This work was supported by resources provided by the Australian Research Council, the Pawsey Supercomputing Centre, and the National Computing Infrastructure of Australia. H.U. acknowledges the contribution of an Australian Government Research Training Program Scholarship.

Appendix A

A.1. Target states of tin

In Table A, all target states of tin for which cross sections are presented are listed. Their calculated excitation energies relative to the ground state are also given alongside comparison with the recommended values of NIST [22]. The NIST values have been rounded to three decimal digits for easier comparisons.

A.2. Optical oscillator strengths

The OOS values presently calculated for all dipole allowed transitions are presented in Table B alongside comparison with accurate calculations of Oliver and Hibbert [27].

Appendix B. Supplementary data

Supplementary material related to this article can be found online at https://doi.org/10.1016/j.adt.2023.101586.

References

[1] A. Foster, G. Counsell, H. Summers, J. Nucl. Mater. 363 (2007) 152.
[2] D.I. Skovorodin, A.A. Pshenov, A.S. Arakcheev, E.A. Eksaeva, E.D. Marenkov, S.I. Krasheninnikov, Phys. Plasmas 23 (2016) 022501.
[3] V. Sizyuk, A. Hassanein, Sci. Rep. 12 (2022) 4698.
[4] P. Rindt, J. van den Eijnden, T. Morgan, N. Lopes Cardozo, Fusion Eng. Des. 173 (2021) 112812.
[5] G. O'Sullivan, B. Li, R. D'Arcy, P. Dunne, P. Hayden, D. Kilbane, T. McCormack, H. Ohashi, F. O'Reilly, P. Sheridan, E. Sokell, C. Suzuki, T. Higashiguchi, J. Phys. B: At. Mol. Opt. Phys. 48 (2015) 144025.
[6] F. Torretti, J. Sheil, R. Schupp, M. Basko, M. Bayraktar, R. Meijer, S. Witte, W. Ubachs, R. Hoekstra, O. Versolato, A. Neukirch, J. Colgan, Nature Commun. 11 (2020).
[7] R. Srivastava, R.P. McEachran, A.D. Stauffer, Can. J. Phys. 80 (2002) 687.
[8] L. Sharma, S. Bharti, R. Srivastava, Eur. Phys. J. D 71 (2017) 121.
[9] R.S. Freund, R.C. Wetzel, R.J. Shul, T.R. Hayes, Phys. Rev. A 41 (1990) 3575.
[10] E.J. McGuire, Phys. Rev. A 16 (1977) 62.
[11] P.L. Bartlett, A.T. Stelbovics, Phys. Rev. A 66 (2002) 012707.
[12] Y.-K. Kim, P.M. Stone, J. Phys. B: At. Mol. Opt. Phys. 40 (2007) 1597.
[13] S. Loch, M. Pindzola, D. Griffin, Int. J. Mass Spectrom. 271 (2008) 68, Yong-Ki Kim Honour Issue.
[14] R. Naghma, B.N. Mahato, M. Vinodkumar, B.K. Antony, J. Phys. B: At. Mol. Opt. Phys. 44 (2011) 105204.
[15] H. Umer, I. Bray, D.V. Fursa, Atoms 10 (2022) 78.
[16] K. Dyall, I. Grant, C. Johnson, F. Parpia, E. Plummer, Comput. Phys. Comm. 55 (1989) 425.
[17] I. Bray, Phys. Rev. A 49 (1994) 1066.
[18] S. Patil, At. Data Nucl. Data Tables 71 (1999) 41.
[19] I.P. Grant, H.M. Quiney, Phys. Rev. A 62 (2000) 022508.
[20] D.V. Fursa, I. Bray, Phys. Rev. A 52 (1995) 1279.
[21] D.V. Fursa, I. Bray, J. Phys. B: At. Mol. Opt. Phys. 30 (1997) 5895.
[22] A. Kramida, Yu. Ralchenko, J. Reader, NIST ASD Team, NIST Atomic Spectra Database (Ver. 5.10), National Institute of Standards and Technology, Gaithersburg, MD, 2022, [Online]. Available: https://physics.nist.gov/asd, [2022, March 1].
[23] C. Thierfelder, B. Assadollahzadeh, P. Schwerdtfeger, S. Schäfer, R. Schäfer, Phys. Rev. A 78 (2008) 052506.
[24] D.V. Fursa, I. Bray, Phys. Rev. Lett. 100 (2008) 113201.
[25] C.J. Bostock, D.V. Fursa, I. Bray, Phys. Rev. A 82 (2010) 022713.
[26] C.J. Bostock, J. Phys. B: At. Mol. Opt. Phys. 44 (2011) 083001.
[27] P. Oliver, A. Hibbert, J. Phys. B: At. Mol. Opt. Phys. 41 (2008) 165003.